Biosensors and Bioelectronics 106 (2018) 43–49

Contents lists available at ScienceDirect

Biosensors and Bioelectronics

journal homepage: www.elsevier.com/locate/bios

Colorimetric and chemiluminescent dual-readout immunochromatographic assay for detection of pesticide residues utilizing g-C_3N_4/$BiFeO_3$ nanocomposites

Hui Ouyang[a,b,1], Xinman Tu[a,c,1], Zhifeng Fu[b], Wenwen Wang[b], Shaofang Fu[a], Chengzhou Zhu[a], Dan Du[a], Yuehe Lin[a,*]

[a] School of Mechanical and Materials Engineering, Washington State University, Pullman, WA 99164, United States
[b] Key Laboratory of Luminescence and Real-Time Analytical Chemistry (Ministry of Education), College of Pharmaceutical Sciences, Southwest University, Chongqing 400716, China
[c] Key Laboratory of Jiangxi Province for Persistent Pollutants Control and Resources Recycle, College of Environmental and Chemical Engineering, Nanchang Hangkong University, Nanchang 330063, China

ARTICLE INFO

Keywords:
Graphitic carbon nitride/bismuth ferrite nanocomposites
Dual-readout
Immunochromatographic assay
Pesticide residues
Chemiluminescence

ABSTRACT

Graphitic carbon nitride/bismuth ferrite nanocomposites (g-C_3N_4/$BiFeO_3$ NCs) were synthesized by a facile one step sol-gel combustion method and employed as a peroxidase-like catalyst. Based on the catalytical activity on the luminol-H_2O_2 reaction, the nanocomposites were utilized as a colorimetric/chemiluminescent dual-readout immunochromatographic assay (ICA) for the multiplexed detection of pesticide residues by utilizing chlorpyrifos and carbaryl as the model analytes. In the proposed protocol, chlorpyrifos antibody and carbaryl antibody were tagged to g-C_3N_4/$BiFeO_3$ NCs for developing the spatially-resolved multianalyte ICA. After two competitive immunoreactions completed on the ICA test strip, the tracer antibodies were captured by the immobilized antigens on two test lines. The accumulation of g-C_3N_4/$BiFeO_3$ NCs led to the appearance of brown color, which were observed as a colorimetric and semi-quantitative signal. Furthermore, the g-C_3N_4/$BiFeO_3$ NCs-driven generation of CL signal was collected as a sensitively quantitative signal after initiating the luminol-H_2O_2 reaction on the test lines. Under the optimal conditions, the limits of detection of chlorpyrifos and carbaryl were both 0.033 ng/mL. The dual-readout ICA was successfully used to detect chlorpyrifos and carbaryl spiked in environmental water and traditional Chinese medicine samples with acceptable recovery values of 80–119% and 90–118%. Due to many advantages including low cost, time efficiency, high sensitivity and good portability, the novel ICA showed great potential in many areas such as drug safety, environmental monitoring and clinical diagnosis.

1. Introduction

The widespread utilization of pesticides has been indispensable to increase the farm productivity in commercial agriculture (Zhang et al., 2014; Hassani et al., 2017; Płonka et al., 2016). However, the tremendous usage results in various unavoidable adverse effects of pesticide residues on human beings, wildlife, traditional Chinese medicines and the environment (Albers et al., 2015; Ellis et al., 2017; Harris et al., 2011; Khairy et al., 2014; Liu et al., 2016; Vasylieva et al., 2015; P. Wang et al., 2017). Maximum residue levels have been set in many countries for regulating pesticide residues and decreasing their harmful impacts. Therefore, it is of great urgency to develop detection methods of time efficiency, high throughout, high sensitivity and improved preciseness for pesticide residues in food safety and environmental monitoring.

In decades, a variety of chromatographic and mass spectrometric protocols have been established for sensitive detection of pesticide residues, including HPLC, HPLC-MS, UPLC-MS and MS-MS (Shi et al., 2014; Vázquez et al., 2016; Watanabe and Baba, 2015; Wittenberg et al., 2014). Due to high sensitivity and preciseness, these instrumental approaches are very fit to be used as confirmatory techniques. However, several limitations such as huge instruments, complicated manipulation and long detection period greatly restrict their application on rapid screening and field detection.

* Corresponding author.
E-mail address: yuehe.lin@wsu.edu (Y. Lin).
[1] Equal contribution

https://doi.org/10.1016/j.bios.2018.01.033
Received 2 October 2017; Received in revised form 3 January 2018; Accepted 15 January 2018
Available online 31 January 2018
0956-5663/

To address the inappropriate situation of these traditional assays, many single-readout nanomaterials-based methods of high throughout and rapid testing have also been developed for detecting pesticide residues (Wen et al., 2017; Wu et al., 2017). Based on the selectively quenching effect of malathion on the peroxidase activity of palladium-gold nanorod, a sensitive colorimetric platform was reported for the pesticide detection. Yan et al. constructed a novel fluorimetric protocol for quantitatively detecting paraoxon via its inhibitory effect on the activity of tyrosinase enzyme for recovering the fluorescence of gold nanocluster (Yan et al., 2017). With a specifically electrocatalytic activity on the hydrolysis of carbaryl, $Au_{42}Rh_{58}$ nanocrystals were utilized for an electrochemical approach of high efficiency to quantitate the carbaryl pesticide (Chen et al., 2017).

Compared with the single-readout analytical strategy, improved exactness and increased sensitivity could be obtained in the dual-readout nanomaterials-based protocols (Liu et al., 2012; Zhang et al., 2015; Zhu et al., 2015). Rhodamine B-functionalized gold nanoparticles were utilized as two probes for organophosphorus and carbamate pesticides in a dual-readout protocol. In the assay procedure, the analytes inhibited the activity of acetylcholinesterase and decreased the generation of thiocholine, which could turn gold the nanoparticles blue while recover the fluorescence of rhodamine B. It is worth noting that in common two individual readout probes were needed to design in this dual-readout strategy, which probably complicated the test process and even led to unexpected interference. Therefore, a single probe with dual-readout performance was distinctly superior to two individual probes in the dual-readout strategy. Moreover, this dual-readout strategy based on the single probe has never been applied to immunochromatographic assay (ICA).

The semi-quantitative ICA possessed such easy manipulation, single step and rapid testing that it was widely utilized in the detection of pesticide residues (Blažková et al., 2010, 2009; Hua et al., 2010); however, its disadvantages of low sensitivity and poor preciseness greatly hindered the further application. Compared with sophisticated instruments in some optical strategies including fluorescence and phosphorescence, there exists no need of expensive excitation source and specialized filter in chemiluminescent (CL) assays. Furthermore, a high signal-to-noise ratio and increased sensitivity could be achieved through CL-based methods (Chen et al., 2016; Lee et al., 2012). Horseradish peroxidase (HRP) was extensively used as catalyst for the generation of strong CL emission of luminol-H_2O_2 system. However, the natural enzyme showed such serious defects as easy denaturation and poor stability. Nowadays, many nanomaterials such as metal nanoparticles (Comotti et al., 2004; Gao et al., 2007; Jiang et al., 2016), carbon nanoparticles (Lin et al., 2014; Qian et al., 2015; Yang et al., 2015; Song et al., 2016; Singh et al., 2017; Zhu et al., 2017), or metal-carbon nanocomposites (Fan et al., 2017; Peng and Weng, 2017; W. Wang et al., 2017) with peroxidase-mimicking activity have been reported as substitutes of HRP in biosensing application. Because of its the perovskite-type structure and Fe element, bismuth ferrite ($BiFeO_3$) has recently been considered as a promising photocatalyst for both the decomposition of H_2O_2 and degradation of organic pollutants (Luo et al., 2010). Graphitic carbon nitride (g-C_3N_4), as a novel and metal-free semiconductor material, has been widely used in catalysis, such as photodegradation of water pollutants (Maeda et al., 2009; Yan et al., 2009), catalysis of organic reactions (Goettmann et al., 2006, 2007) and electrocatalysis for oxygen reduction reaction (Zhai et al., 2013). As predicted, enhanced photocatalytic activity has been obtained by combining g-C_3N_4 with $BiFeO_3$ for decomposing organic compounds (Fan et al., 2015; Wang et al., 2015). Such photocatalysts integrating the synergistic effects of the individual species, which could endow the composite systems with increased visible light harvesting ability, improved separation efficiency of photogenerated electron–hole pairs, and prolonged lifetime of carriers, thereby resulting in the enhanced photocatalytic activity. Because $BiFeO_3$ and g-C_3N_4 have good catalytic ability, we anticipate that g-C_3N_4/$BiFeO_3$ nanocomposites (g-C_3N_4/$BiFeO_3$ NCs) are a powerful candidate for a peroxidase. To the best of our knowledge, g-C_3N_4/$BiFeO_3$ NCs have not reported as a single peroxidase-like probe to fabricate dual-readout ICA so far.

Herein, g-C_3N_4/$BiFeO_3$ NCs were synthesized by a facile one step sol-gel combustion method and used as a peroxidase-mimicking CL catalyst for developing a dual-readout ICA for the multiplexed detection of pesticide residues, by adopting chlorpyrifos and carbaryl as the model analytes. Chlorpyrifos antibody and carbaryl antibody were tagged to g-C_3N_4/$BiFeO_3$ NCs as spatially-resolved probes. After the tracer antibodies were captured by the immobilized antigens on test lines, brown colors of g-C_3N_4/$BiFeO_3$ NCs and the g-C_3N_4/$BiFeO_3$-driven CL signal were collected as qualitative and quantitative readouts in the proposed protocol. The new dual-readout ICA opened a new avenue for multiplexed detection of pesticide residues by using a peroxidase-like nanomaterial as single probe.

2. Experimental

2.1. Instruments

CL measurements were carried out using a MPI-A CL analyzer (Xi'an Remax Electronic Science & Technology Co., Ltd., China) equipped with a photomultiplier operated at −800 V. Powder X-ray diffraction (XRD) was performed on a Bruker D8-Advance X-ray diffractometer with monochromatized Cu Kα radiation (λ = 1.5418 Å). Scanning electron microscopy (SEM) using a JEOL JSM-6700F FESEM was employed for the morphological characterization. Transmission electron microscopy (TEM) images were taken with a JEOL JEM-1010 transmission electron microscope operated at 120 kV. Fourier transform infrared (FTIR) spectra were performed using Perkin-Elmer spectrometer in the frequency range of 4000–400 cm^{-1} with a resolution of 4 cm^{-1}. Ultrapure water (18.2 MΩ/cm) by a Milli-Q Integral system (Millipore) was utilized for preparing all aqueous solutions.

2.2. Reagents and materials

TMB Liquid Substrate System, melamine, $Bi(NO_3)_3{\cdot}5H_2O$, $Fe(NO_3)_3{\cdot}9H_2O$, chlorpyrifos, carbaryl, parathion, methyl parathion, fenitrothion, aldicarb, methomyl and fenoxycarb were all obtained from Sigma-Aldrich (USA). Mouse monoclonal antibody for chlorpyrifos (chlorpyrifos antibody), mouse monoclonal antibody for carbaryl (carbaryl antibody), chlorpyrifos-BSA bioconjugate and carbaryl-BSA bioconjugate were all purchased from Wuxi Determine Bio-Tech Co. Ltd. (China). Goat anti-mouse IgG was purchased from Boster Biotechnology Co., Ltd. (China). The ICA test strips including nitrocellulose membrane, sample pad, conjugate pad and absorbent pad were provided by Millipore Corp. (USA). 0.10 M phosphate buffer saline (PBS) at pH 7.4 containing 1.0% BSA and 0.05% Tween-20 was prepared as a blocking buffer for the pretreatment of the conjugate pad and sample pad prior to use. Polystyrene 96-well microplates were obtained from Corning Incorporated (USA). *Salvia miltiorrhiza* and *Codonopsis pilosula* were purchased from a pharmacy in Chongqing (China) and the lake water was collected from the Wawawai lake (USA).

2.3. Preparation of g-C_3N_4 powders, $BiFeO_3$ powders and g-C_3N_4/$BiFeO_3$ NCs

The g-C_3N_4 powders were obtained by directly heating melamine at 550 °C in a muffle furnace for 3 h at a heating rate of 5 °C/min in a semiclosed alumina crucible with a cover, and the further deammoniation treatment was set at this temperature for another 3 h. After cooling to room temperature (RT), the products were collected and ground into yellow powders.

g-C_3N_4/$BiFeO_3$ NCs were fabricated by sol–gel combustion synthesis process. In a typical process, stoichiometric $Bi(NO_3)_3{\cdot}5H_2O$ and Fe

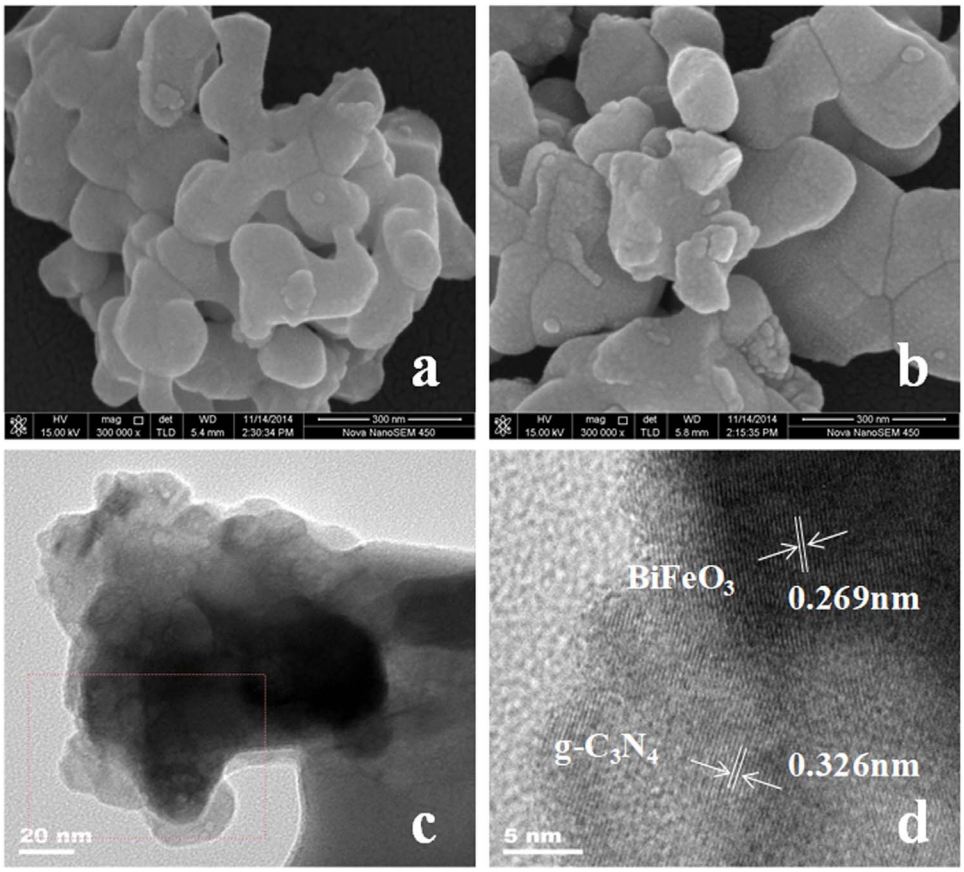

Fig. 1. SEM of $BiFeO_3$ (a) and g-C_3N_4/$BiFeO_3$ NCs (b), TEM (c) and HRTEM (d) of g-C_3N_4/$BiFeO_3$ NCs.

$(NO_3)_3$·$9H_2O$ (10 mmol) were dissolved into 2-methoxyethanol (50 mL) under magnetic stirring. A stable transparent sol was formed and then slowly added 10 mmol melamine continuously stirred for 30 min under 80 °C to completely dissolve melamine. Then the solution was heated at 120 °C until a fluffy dried gel was obtained. The resultant dried gel was transferred to a crucible, and preheated to 350 °C for 30 min at a heating rate of 5 °C/min to remove organic compounds and NO_3^-. Then the finely ground powders were loaded into the furnace maintained at 550 °C for 30 min before directly quenching to RT in air. Finally, the as-prepared g-C_3N_4/$BiFeO_3$ NCs was washed repeatedly with deionized water for several times, centrifuged at 11,000 g for 10 min, and vacuum-dried at 60 °C. As a comparison, pure $BiFeO_3$ counterpart was synthesized without the addition of melamine under the same process.

2.4. Preparation of g-C_3N_4/$BiFeO_3$ NCs-modified antibodies

Similar to a previous report (Ding et al., 2016), the conjugate of g-C_3N_4/$BiFeO_3$ NCs-labeled chlorpyrifos antibody and g-C_3N_4/$BiFeO_3$ NCs-labeled carbaryl antibody were successfully prepared. In detail, 2.0 mg of the g-C_3N_4/$BiFeO_3$ NCs was dispersed in 1.0 mL ultrapure water and continuously ultrasonicated in a water bath for 30 min. Afterward, the solution was then centrifuged at 425 g for 10 min to remove the large particles. The g-C_3N_4/$BiFeO_3$ NCs solution was adjusted to pH 8.5–9.0 with 0.02 M K_2CO_3. Then 10 μL of 1 mg/mL antibody was added into the adjusted solution for a 60-min incubation with a gentle shaking at RT. Subsequently, 220 μL of 10% BSA was added into the mixture, followed by another incubation for 30 min. Lastly, the mixed solution was centrifuged at 10,610 g for 10 min and washed twice with 2% BSA. The obtained precipitation was re-suspended in 200 μL of ultrapure water containing 2% BSA and 3% sucrose and stored in 4 °C for the detection of pesticide residues.

2.5. Fabrication of dual-readout ICA test strip

The ICA test strip (4 mm in width) consists of sample pad, conjugate pad, nitrocellulose membrane and absorbent pad. The sample pad and the conjugate pad were blocked with the blocking buffer and dried at 37 °C for 2 h. The mixture of g-C_3N_4/$BiFeO_3$ NCs-labeled antibodies was deposited on the treated conjugate pad and dried at 37 °C. Then 0.5 μL of carbaryl-BSA conjugate, 0.5 μL of chlorpyrifos-BSA conjugate and 0.5 μL of 1.0 mg/mL goat anti-mouse IgG were dispensed on the desired sites on the nitrocellulose membrane to form test line 1 (T1), test line 2 (T2) and control line, respectively, followed by overnight incubation at 4 °C. Finally, 1.5 mm overlap between every two adjacent parts of ICA test strip should be achieved when assembled.

2.6. Dual-readout assay procedure

A sample solution (80 μL) containing chlorpyrifos and carbaryl was added onto the sample pad and migrated to the absorbent pad under the force of capillary action. After two competitive immunoreactions occurred on test lines, brown color was observed by bare eyes as colorimetric and semi-quantitative readouts. After that, the test lines were cut and put into two microplate wells containing luminol solution as CL emitter (50 μL/well). Subsequently, freshly prepared H_2O_2 was utilized as the CL coreactant and injected into the wells (50 μL/well) for triggering the CL reactions. Finally, CL signals from the wells were recorded as quantitative readouts for detecting chlorpyrifos and carbaryl.

2.7. Preparation of mock samples

After a desired amount of two analytes (dissolved in methanol) was mixed thoroughly with 1.0 g of the ground *Salvia miltiorrhiza* or *Codonopsis pilosula*, 10 mL of PBS (0.10 M, pH 7.4) containing 0.05% Tween-20% and 10% methanol was used to extract the spiked

pesticides, followed by a vortex stirring for 15 min at RT. The mixture containing pesticides was centrifuged at 5200 g for 5 min, and then the supernatant was diluted to a desired amount. For the lake water sample, it was pretreated with a 0.22 μm-sized filter membrane for further use.

3. Results and discussion

3.1. Characteristics of g-C_3N_4/$BiFeO_3$ NCs

Based on the facile one step sol-gel combustion method with high reproducibility, the g-C_3N_4/$BiFeO_3$ nanocomposites at gram level could be easily synthesized once. XRD patterns and the FTIR spectra of g-C_3N_4/$BiFeO_3$ NCs clearly revealed the coexistence of the g-C_3N_4 and the $BiFeO_3$ phases, and no other impurity phases formed in the composites, showing that one step sol–gel combustion method was feasible (see XRD and FTIR spectra, Figs. S1 and S2, respectively). Fig. 1a and b showed the SEM images of pure $BiFeO_3$ and g-C_3N_4/$BiFeO_3$ composite samples. As can be seen, $BiFeO_3$ and g-C_3N_4/$BiFeO_3$ composite samples had the same morphology and were all an agglomeration structure, nothing but the surface of g-C_3N_4/$BiFeO_3$ NCs were rougher than that of $BiFeO_3$. The microstructure of g-C_3N_4/$BiFeO_3$ NCs were studied by TEM and HRTEM, as shown in Figs. 1c and 1d. As can be seen from Fig. 1c, the $BiFeO_3$ particle was surrounded by g-C_3N_4 shells. In Fig. 1d, the interplanar spacing of 0.326 nm corresponded the (002) crystal plane of g-C_3N_4, while the other of 0.269 nm corresponded the (110) crystal plane of $BiFeO_3$ particle, indicating well developed nanocrystallites of $BiFeO_3$ and g-C_3N_4 in the composites. Based on the above results, it indicated that heheterojunction structure indeed formed from the two materials, which facilitated the charge transfer and improves the CL performance.

3.2. Peroxidase-like catalytical activity of g-C_3N_4/$BiFeO_3$ NCs on CL emission

In this investigation, the peroxidase-mimicking activity of g-C_3N_4/$BiFeO_3$ NCs was estimated by studying its enhancing effect on luminol-H_2O_2 CL emission. As seen in Fig. 2, CL signals enhanced by g-C_3N_4 powder, $BiFeO_3$ powder and g-C_3N_4/$BiFeO_3$ NCs all at 2 mg/mL were observed 6.6, 2.9 and 33.2 times, respectively, of that by ultrapure water (as blank). The results indicated the g-C_3N_4 powder, the $BiFeO_3$ powder and the g-C_3N_4/$BiFeO_3$ NCs showed enzyme-like activity on luminol-H_2O_2 CL system. Furthermore, the enhancing effect of g-C_3N_4/$BiFeO_3$ NCs was superior to that of a mixture of two individual ingredients (at a mass ratio of 1:1), implying the g-C_3N_4/$BiFeO_3$ NCs

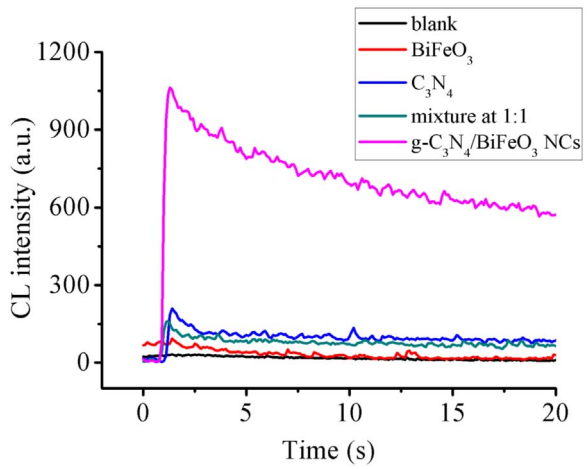

Fig. 2. CL signals enhanced by g-C_3N_4 powder, $BiFeO_3$ powder, g-C_3N_4/$BiFeO_3$ NCs and a mixture of g-C_3N_4 powder, $BiFeO_3$ powder (at a mass ratio of 1:1), where the concentrations of luminol, H_2O_2 and nanomaterials were 5×10^{-7} M, 20 mM and 2 mg/mL, respectively.

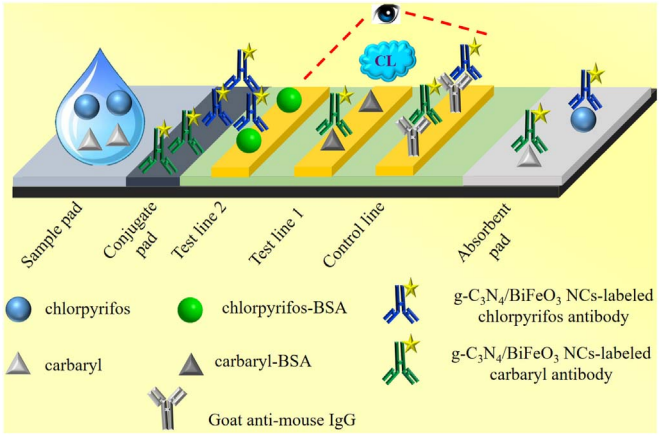

Fig. 3. Schematic illustration of the dual-readout ICA for multiplexed detection of chlorpyrifos and carbaryl.

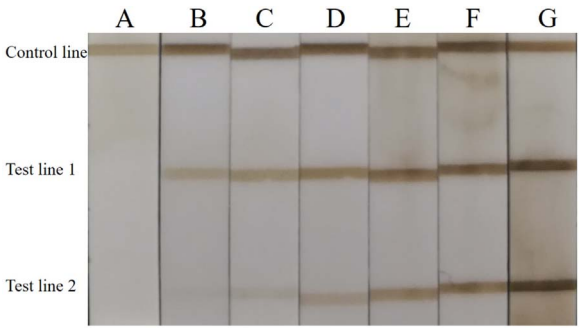

Fig. 4. Photographs of visual readout of the proposed ICA for the detections of carbaryl (test line 1) and chlorpyrifos (test line 2) both at (A) 100, (B) 50, (C) 20, (D) 10, (E) 5.0, (F) 0.1 and (G) 0 ng/mL.

displayed a collaborative effect on the catalytical activity on CL emission compared with the individual usage of g-C_3N_4 powder and $BiFeO_3$ powder. The prepared nanocomposites were found to remain stable for 6 months without the loss of the catalytic activity when stored at RT.

As such TMB–H_2O_2 coloration tests were also conducted to explore the peroxidase-like catalytical activity of g-C_3N_4/$BiFeO_3$ NCs. As seen in Fig. S3, g-C_3N_4/$BiFeO_3$ NCs could catalyze H_2O_2-induced TMB oxidation within 1 min. The possible CL mechanism of g-C_3N_4/$BiFeO_3$ NCs-driven luminol could be described as follows (Jiang et al., 2017):

$$g\text{-}C_3N_4 + H_2O_2 \rightarrow g\text{-}C_3N_4^{-} + OH^{\bullet} + OH^{-}$$

$$FeO_3^{3-} + H_2O_2 \rightarrow FeO_3^{4-} + OH^{\bullet} + OH^{-}$$

$$LH + OH^{\bullet} \rightarrow LH^{\bullet}$$

$$LH^{\bullet} \rightarrow L^{\bullet-} + H^{+}$$

$$L^{\bullet-} + H_2O_2 \rightarrow L + O_2^{\bullet-}$$

$$L^{\bullet-} + O_2^{\bullet-} + H^{+} \rightarrow LOOH^{-}$$

$$LOOH^{-} \rightarrow aminophthalate + N_2 + h\nu$$

Herein, based on the peroxidase-like catalytical activity of g-C_3N_4/$BiFeO_3$ NCs, H_2O_2 was oxidized to yield reactive oxygen species ($OH^{\bullet}$). Then, luminol (LH) reacted with reactive oxygen species for generating excited aminophthalate, which returned to the ground state to emit light.

3.3. Principle of dual-readout ICA

As shown in Fig. 3, sample solution containing chlorpyrifos and carbaryl was deposited onto the sample pad and then diffused towards

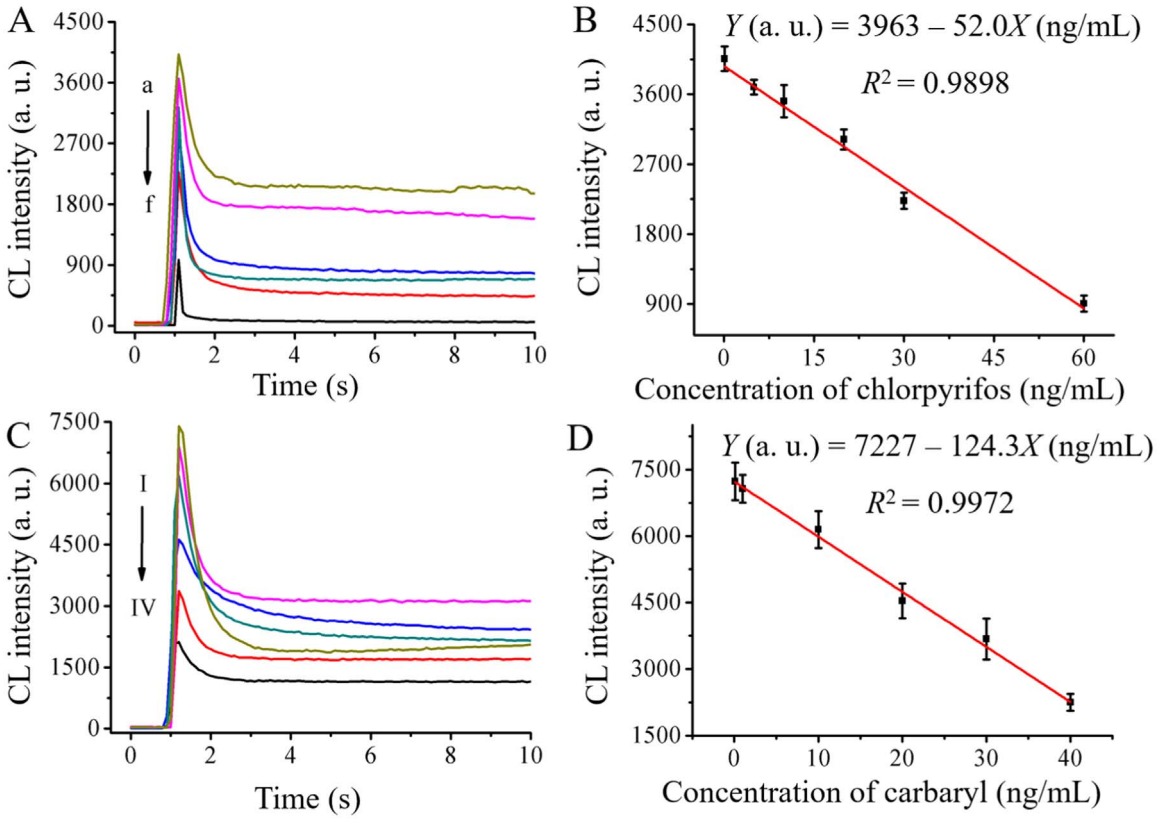

Fig. 5. (A) CL responses of the present ICA for the detection of chlorpyrifos at (a) 0.1, (b) 5.0, (c) 10, (d) 20, (e) 30 and (f) 60 ng/mL. (B) Calibration curve for CL detection of chlorpyrifos. (C) CL responses of the present ICA for the detection of carbaryl at (I) 0.1, (II) 1.0, (III) 10, (IV) 20, (V) 30 and (VI) 40 ng/mL. (D) Calibration curve for CL detection of carbaryl. All the tests were conducted under the optimal conditions, $n = 3$.

Table 1
Recovery tests of chlorpyrifos (A) and carbaryl (B) spiked in *Salvia miltiorrhiza* and *Codonopsis pilosula* and lake water ($n = 3$).

	Salvia miltiorrhiza samples						*Codonopsis pilosula* samples						lake water samples					
	A	B	A	B	A	B	A	B	A	B	A	B	A	B	A	B	A	B
Added (ng/mL)	1.0	1.0	10	10	30	30	1.0	1.0	10	10	30	30	1.0	1.0	10	10	30	30
Found (ng/mL)	0.8	1.1	11.9	11.4	27.8	35.4	1.0	0.9	10.1	11.1	25.0	35.4	1.0	1.0	10.5	10.7	32.5	35.3
RSD (%)	6.8	5.9	9.6	7.0	8.7	6.7	7.7	5.2	3.3	2.3	6.4	7.4	3.6	6.6	6.4	1.9	2.7	4.7
Recovery (%)	80	110	119	114	93	118	100	90	101	111	83	118	100	100	105	107	108	118

the absorbent pad by the drive of capillary force. In the meanwhile, the sample solution migrated with g-C_3N_4/$BiFeO_3$ NCs-modified antibodies on the conjugated pad. As the mixture of analytes and the tracer antibodies arrived on the test lines, the immobilized antigens competed with their corresponding analytes for binding with the tracer antibodies. After two competitive immunoreactions completed, the accumulation of captured g-C_3N_4/$BiFeO_3$ NCs on two test lines resulted in the appearance of brown color, which was observed by naked eyes for the visual and semi-quantitative detection of pesticide residues. Afterward the CL responses enhanced by the captured g-C_3N_4/$BiFeO_3$ NCs were recorded for sensitively detecting the analytes.

3.4. Optimization of the assay conditions

Optimization tests of some assay conditions such as the volume of g-C_3N_4/$BiFeO_3$ NCs-modified antibodies, the incubation time, the pH value and concentrations of CL reagents were conducted to achieve good analytical performance of the dual-readout ICA. In detail, CL signals from different volumes of tracer antibodies were collected for the analytes (as signal) and PBS (as blank) for studying the optimal volumes of tracer antibodies. In the investigation, chlorpyrifos and carbaryl both at 25 ng/mL were adopted. As seen in Figs. S4A and S4B, when 5.0 and 7.0 μL were adopted as the volumes of the tracer antibodies for chlorpyrifos and carbaryl, respectively, the signal-to-blank ratios reached the minimal values of 74.2% and 64.4%. It indicated that the competitive immunoreactions between the free analytes and the immobilized antigens on the test lines were both the strongest. For the optimization of the incubation time, as seen in Figs. S4C and S4D, the CL signals increased obviously with an increasing incubation time and almost reached to the maximal value at 10 min, suggesting the immunobinding tended to the saturation under the condition. In the optimization tests of the CL emission condition, a strong response could be obtained in 0.10 M carbonate buffer saline at pH 9.5 and thus it was adopted as the medium for the CL system (data not shown). Similarly, the optimal concentrations of luminol and H_2O_2 were chosen to be 5.0×10^{-5} M and 20 mM (data not shown), respectively.

3.5. Analytical performance of dual-sensing ICA

As seen in Fig. 4, brown color on two test lines faded with the increase of analyte concentrations since a competitive immunoassay mode was performed. Due to the easily semi-quantitative detection of

pesticide residues using a visual readout, the present ICA showed great potential in field assay and rapid screening compared with other instrumental techniques. Additionally, the sensors in smartphones could also be utilized as facile colorimetric detectors in the proposed ICA for semi-quantitating the analytes, which was probably of great use for the future application of the present device (Vashist et al., 2014).

Similarly, the luminol-H_2O_2 CL signals-driven by the g-C_3N_4/$BiFeO_3$ NCs decreased with the concentrations of chlorpyrifos and carbaryl (Fig. 5). The linear ranges of chlorpyrifos and carbaryl were 0.1–60 ng/mL and 0.1–40 ng/mL, respectively. The detection ranges of chlorpyrifos and carbaryl were 1.0–60 ng/mL and 1.0–40 ng/mL, respectively. The limits of detection of two analytes were both 0.033 ng/mL and the limits of quantification of two analytes were both 1.0 ng/mL. The regression equations for chlorpyrifos and carbaryl could be expressed as Y (a. u.) = 3963 – 52.0X (ng/mL) (R^2 = 0.9898) and Y (a. u.) = 7227 – 124.3X (ng/mL) (R^2 = 0.9972), respectively, where Y was the signal intensity and X was the concentration of chlorpyrifos or carbaryl. The reproducibility of the proposed protocol was estimated through the relative standard deviation (RSD) values for the analytes at high (20 ng/mL), medium (10 ng/mL), low concentrations (0.1 ng/mL). The RSD values for two analytes were not higher than 8.6%, implying the good reliability of the proposed method. Owing to several merits including one step, easy operation, fast response, dual readout and low assay cost, the proposed dual-readout method was also utilized as a potential technique for point of care detection of pesticide residues (Vashist et al., 2015).

3.6. Estimation of specificity the ICA

The specificity tests of the ICA were conducted by detecting the CL signals caused by some chemical compounds with similar structures of chlorpyrifos or carbaryl. In detail, parathion, methyl parathion and fenitrothion were adopted as the interferents of chlorpyrifos, while aldicarb, methomyl and fenoxycarb were adopted as the interferents of carbaryl. In the specificity investigation, pesticides all at 20 ng/mL were adopted. The degree of interference values were calculated through the following equation:

$$\text{Degree of interference} = \frac{|B\text{-}I|}{B\text{-}T} \times 100\% \quad (1)$$

Here, B, I and T represent the CL signals resulting from the blank (PBS), interferents and analytes. As seen in Fig. S5, the degree of interference values for chlorpyrifos and carbaryl, respectively, were not higher than 8.0% and 8.1%, indicating the satisfying selectivity of the ICA for the detection of chlorpyrifos and carbaryl.

3.7. Mock sample test

For estimating the application potential of the present ICA, *Salvia miltiorrhiza* and *Codonopsis pilosula* and lake water were spiked with two analytes to perform mock sample test. The recovery values of chlorpyrifos and carbaryl displayed in Table 1 were 80–119% and 90–118%, respectively, with all RSD values not higher than 9.6%, which demonstrated the reliability of the ICA for multiplexed detection of pesticide residues in the traditional Chinese medicine and environmental water samples.

4. Conclusion

The g-C_3N_4/$BiFeO_3$ NCs were synthesized and adopted as a peroxidase-mimicking nanoprobe to develop a dual-readout ICA for the multiplexed detection of chlorpyrifos and carbaryl. Compared with g-C_3N_4 power and $BiFeO_3$ power, the g-C_3N_4/$BiFeO_3$ NCs showed a significantly collaborative catalytical activity on the CL emission of luminol-H_2O_2 system. Superior to the previously joint usage of two individual signal performing two readouts, the g-C_3N_4/$BiFeO_3$ NCs with a dual-sensing feature was utilized as a unique colorimetric/CL for simultaneously semi-quantitative and high-sensitive detection of pesticide residues. The successful application of the present ICA on mock samples demonstrated its great potential on drug safety and environmental monitoring, showing the good practicability of the dual-sensing peroxidase-like nanomaterials-based immunoassay.

Acknowledgements

This research was financially supported by the Centers for Disease Control and Prevention/National Institute for Occupational Safety and Health (CDC/NIOSH) Grant No. R01OH011023-01A1. Its contents are solely the responsibility of the authors and do not necessarily represent the official views of CDC. H. Ouyang acknowledged the financial support from the China Scholarship Council Grant No. 201606990032.

Appendix A. Supporting information

Supplementary data associated with this article can be found in the online version at http://dx.doi.org/10.1016/j.bios.2018.01.033.

References

Albers, C.N., Feld, L., Ellegaard-Jensen, L., Aamand, J., 2015. Water Res. 83, 61–70.
Blažková, M., Mičková-Holubová, B., Rauch, P., Fukal, L., 2009. Biosens. Bioelectron. 25, 753–758.
Blažková, M., Rauch, P., Fukal, L., 2010. Biosens. Bioelectron. 25, 2122–2128.
Chen, W., Liu, Y., Zhang, Y., Fang, J., Xu, P., Xu, J., Li, X., Liu, C.-C., Wen, W., 2017. J. Mater. Chem. A 5, 7064–7071.
Chen, Y., Sun, J., Xianyu, Y., Yin, B., Niu, Y., Wang, S., Cao, F., Zhang, X., Wang, Y., Jiang, X., 2016. Nanoscale 8, 15205–15212.
Comotti, M., Della Pina, C., Matarrese, R., Rossi, M., 2004. Angew. Chem. Int. Ed. 43, 5812–5815.
Ding, L.-L., Ge, J.-P., Zhou, W.-Q., Gao, J.-P., Zhang, Z.-Y., Xiong, Y., 2016. Biosens. Bioelectron. 85, 212–219.
Ellis, C., Park, K.J., Whitehorn, P., David, A., Goulson, D., 2017. Environ. Sci. Technol. 51 (3), 1727–1732 (2017).
Fan, S., Zhao, M., Ding, L., Li, H., Chen, S., 2017. Biosens. Bioelectron. 89, 846–852.
Fan, T., Chen, C., Tang, Z., Ni, Y., Lu, C., 2015. Mater. Sci. Semicond. Process. 40, 439–445.
Gao, L., Zhuang, J., Nie, L., Zhang, J., Zhang, Y., Gu, N., Wang, T., Feng, J., Yang, D., Perrett, S., 2007. Nat. Nanotechnol. 2, 577–583.
Goettmann, F., Fischer, A., Antonietti, M., Thomas, A., 2006. Chem. Commun. 4530–4532.
Goettmann, F., Fischer, A., Antonietti, M., Thomas, A., 2007. New J. Chem. 31, 1455–1460.
Harris, E.S.J., Cao, S.G., Littlefield, B.A., Craycroft, J.A., Scholten, R., Kaptchuk, T., Fu, Y.L., Wang, W.Q., Liu, Y., Chen, H.B.A., Zhao, Z.Z., Clardy, J., Woolf, A.D., Eisenberg, D.M., 2011. Sci. Total Environ. 409, 4297–4305.
Hassani, S., Momtaz, S., Vakhshiteh, F., Maghsoudi, A.S., Ganjali, M.R., Norouzi, P., Abdollahi, M., 2017. Arch. Toxicol. 91, 109–130.
Hua, X., Qian, G., Yang, J., Hu, B., Fan, J., Qin, N., Li, G., Wang, Y., Liu, F., 2010. Biosens. Bioelectron. 26, 189–194.
Jiang, J., Chen, D., Du, X., 2017. Sens. Actuators B 251, 256–263.
Jiang, T., Song, Y., Wei, T., Li, H., Du, D., Zhu, M., Lin, Y., 2016. Biosens. Bioelectron. 77, 687–694.
Khairy, M., Muir, D., Teixeira, C., Lohmann, R., 2014. Environ. Sci. Technol. 48, 9315–9324.
Lee, J.S., Joung, H.-A., Kim, M.-G., Park, C.B., 2012. ACS Nano 6, 2978–2983.
Lin, T., Zhong, L., Wang, J., Guo, L., Wu, H., Guo, Q., Fu, F., Chen, G., 2014. Biosens. Bioelectron. 59, 89–93.
Liu, D., Chen, W., Wei, J., Li, X., Wang, Z., Jiang, X., 2012. Anal. Chem. 84, 4185–4191.
Liu, X., Shen, Z., Wang, P., Liu, C., Yao, G., Zhou, Z., Liu, D., 2016. Environ. Sci. Technol. 50, 5695–5701.
Luo, W., Zhu, L., Wang, N., Tang, H., Cao, M., She, Y., 2010. Environ. Sci. Technol. 44, 1786–1791.
Maeda, K., Wang, X., Nishihara, Y., Lu, D., Antonietti, M., Domen, K., 2009. J. Phys. Chem. C 113, 4940–4947.
Peng, J., Weng, J., 2017. Biosens. Bioelectron. 89, 652–658.
Płonka, M., Walorczyk, S., Miszczyk, M., 2016. Trends Anal. Chem. 85, 67–80.
Qian, J., Yang, X., Yang, Z., Zhu, G., Mao, H., Wang, K., 2015. J. Mater. Chem. B 3, 1624–1632.
Shi, Z., Hu, J., Li, Q., Zhang, S., Liang, Y., Zhang, H., 2014. J. Chromatogr. A 1355, 219–227.
Singh, S., Mitra, K., Shukla, A., Singh, R., Gundampati, R.K., Misra, N., Maiti, P., Ray, B., 2017. Anal. Chem. 89, 783–791.
Song, Y., Luo, Y., Zhu, C., Li, H., Du, D., Lin, Y., 2016. Biosens. Bioelectron. 76, 195–212.
Vashist, S.K., Mudanyali, O., Schneider, E.M., Zengerle, R., Ozcan, A., 2014. Anal. Bioanal. Chem. 406, 3263–3277.

Vashist, S.K., Luppa, P.B., Yeo, L.Y., Ozcan, A., Luong, J.H.T., 2015. Trends Biotechnol. 33, 692–705.
Vasylieva, N., Ahn, K.C., Barnych, B., Gee, S.J., Hammock, B.D., 2015. Environ. Sci. Technol. 49, 10038–10047.
Vázquez, P.P., Hakme, E., Uclés, S., Cutillas, V., Galera, M.M., Mughari, A.R., Fernandez-Alba, A.R., 2016. J. Chromatogr. A 1463, 20–31.
Wang, P., Wu, L., Lu, Z., Li, Q., Yin, W., Ding, F., Han, H., 2017. Anal. Chem. 89, 2424–2431.
Wang, W., Bao, T., Zeng, X., Xiong, H., Wen, W., Zhang, X., Wang, S., 2017. Biosens. Bioelectron. 91, 183–189.
Wang, X., Mao, W., Zhang, J., Han, Y., Quan, C., Zhang, Q., Yang, T., Yang, J., Huang, W., 2015. J. Colloid Interface Sci. 448, 17–23.
Watanabe, E., Baba, K., 2015. J. Chromatogr. A 1385, 35–41.
Wen, W., Yan, X., Zhu, C., Du, D., Lin, Y., 2017. Anal. Chem. 89, 138–156.
Wittenberg, J.B., Zhou, W., Wang, P.G., Krynitsky, A.J., 2014. J. Chromatogr. A 1359, 140–146.
Wu, X., Song, Y., Yan, X., Zhu, C., Ma, Y., Du, D., Lin, Y., 2017. Biosens. Bioelectron. 94, 292–297.
Yan, S., Li, Z., Zou, Z., 2009. Langmuir 25, 10397–10401.
Yan, X., Li, H., Hu, T., Su, X., 2017. Biosens. Bioelectron. 91, 232–237.
Yang, G., Zhu, C., Du, D., Zhu, J., Lin, Y., 2015. Nanoscale 7, 14217–14231.
Zhai, H., Cao, L., Xia, X., 2013. Chin. Chem. Lett. 24, 103–106.
Zhang, R., Li, N., Sun, J., Gao, F., 2015. J. Agric. Food Chem. 63, 8947–8954.
Zhang, W., Asiri, A., Liu, D., Du, D., Lin, Y., 2014. Trends Anal. Chem. 54, 1–10.
Zhu, C., Du, D., Lin, Y., 2015. 2D Mater. 2 (3), 032004.
Zhu, C., Du, D., Lin, Y., 2017. Biosens. Bioelectron. 89, 43–55.